

# Design, Synthesis, Evaluation, and Molecular Docking Study of Ascorbic Acid Dual-Coated Omeprazole Pellets and the Antioxidative Effect of Ascorbic Acid on Omeprazole-Induced Renal Injury in an Animal Model

Hina Raza, Ali Abrar, Asmara Ashraf, Suryyia Manzoor, Rahat Shamim, Farhan Siddique,\*  
Ahmad Mohammad Salamatullah, Mohammed Bourhia, and Gezahign Fentahun Wondmie\*



Cite This: *ACS Omega* 2024, 9, 1143–1155



Read Online

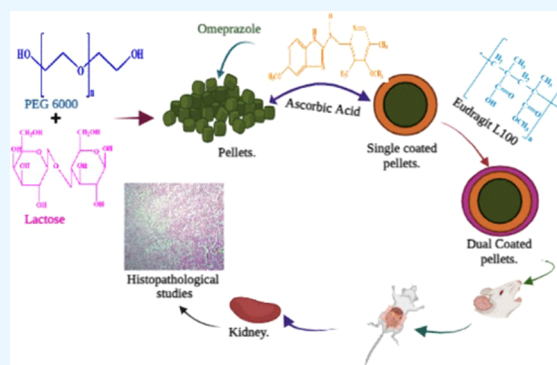
ACCESS |

Metrics & More

Article Recommendations

Supporting Information

**ABSTRACT:** The present study was carried out to investigate the antioxidant effect of ascorbic acid on omeprazole (O.P.)-induced acute kidney infection (AKI). Design of experiment (DoE) was employed to fabricate formulations (P1–P8) by the extrusion spheronization technique, and they were evaluated using various analytical techniques. P1–P8 formulations have % drug loading ranging from  $56.34 \pm 1.10$  to  $98.67 \pm 1.05\%$ , encapsulation efficiency from  $70.98 \pm 0.96$  to  $98.67 \pm 1.05\%$ , percentage drug release varying from  $36.56 \pm 1.34$  to  $93.45 \pm 1.45\%$ , Hausner's ratio ranging from  $1.026 \pm 0.05$  to  $1.065 \pm 0.02\%$ , and Carr's index varying from  $2.3 \pm 0.07$  to  $6.1 \pm 0.06$  g/mL. The optimized formulation (P6) was dual-coated with Eudragit L-100 (5% w/v) and ascorbic acid (2% w/v). A smooth uniform morphology was found after coating, and particle size nonsignificantly changed from  $85.31 \pm 77.43$  to  $101.99 \pm 65.56$   $\mu\text{m}$ . IR spectra showed omeprazole characteristic peaks confirming drug loading, and peaks at 1747.40 and 1611.51  $\text{cm}^{-1}$  confirmed ascorbic acid and Eudragit L-100 coating. X-ray diffraction (XRD) analysis confirmed the crystalline nature, and thermal degradation studies until 500 °C demonstrated increased stability after coating. Cytotoxicity analysis with 97% cell viability revealed the nontoxic behavior of pellets. *In vitro* dissolution studies of coated pellets showed <20% drug release at pH 1.2 and 99.54% at pH 6.8. Animal studies showed that pure omeprazole showed a nonsignificant decrease in weight, urine output, and fecal output compared to rodents on ascorbic acid pellets. Increased uric acid and creatinine levels in the group on pure omeprazole indicated AKI. Histopathological studies of renal cells also supported these results. The integration of experimental pellet formulation with molecular docking simulations has unveiled the potential of ascorbic acid and omeprazole as highly promising therapeutic agents for addressing oxidative stress and inflammation.



## 1. INTRODUCTION

Proton pump inhibitors (PPIs) have extensive therapeutic use in veterinary and human medicine. PPIs constrain gastric acid secretion by  $\text{H}^+/\text{K}^+$ -ATPase blocking in gastric parietal cells. Omeprazole is a commonly used PPI prescribed for its therapeutic value against gastroesophageal reflux disease and peptic ulcer disease as well as intercepting the adverse effects of nonsteroidal anti-inflammatory drugs. Omeprazole suppresses the  $\text{H}^+/\text{K}^+$ -ATPase system in gastric parietal cells, thus hampering acid secretion.<sup>1</sup> Omeprazole causes acute kidney infection (AKI) due to acute tubulointerstitial nephritis (AIN), particularly in elderly patients.

Furthermore, recent independent PPI consumption-related studies have proven that it increases the risk of chronic kidney disease (CKD) by elevating the mitochondrial and cytosolic reactive oxygen species (ROS) levels, which leads to a rise in lipid peroxidation, lysosomal pH, massive vacuolization, and in

turn necrotic tubular cell death and increased serum creatinine.<sup>2</sup> According to the FDA Adverse Event Reporting System (FAERS) database, 3187 PPI cases associated with AKI were identified from January 2004 to December 2019.<sup>3</sup> In the recent era, remarkable evolution in the domain of polymeric drug delivery systems has contributed to various areas from improvising pharmacokinetic profiles to solving toxicity problems. Additionally, applying various coating solutions on the dosage form surface has proven promising to cope with release profiles and adverse effect-related problems. In coating

**Received:** September 25, 2023

**Revised:** November 30, 2023

**Accepted:** December 4, 2023

**Published:** December 19, 2023



**Table 1. Drug Loading, Encapsulation Efficiency, and Drug Release of Different Formulations**

formulation	PEG 6000 (mg)	lactose (mg)	avicel PH 102 (mg)	omeprazole (mg)	drug loading (%)	encapsulation efficiency (%)	drug release (%)
P1	5	30	10	20	56.34 ± 1.10	76.78 ± 1.34	36.56 ± 1.34
P2	10	30	10	20	67.98 ± 1.09	70.98 ± 0.96	47.45 ± 0.45
P3	15	30	10	20	74.76 ± 1.07	75.56 ± 1.54	57.89 ± 1.54
P4	15	10	50	20	87.34 ± 2.15	83.76 ± 2.34	78.56 ± 1.03
P5	15	30	50	20	80.56 ± 2.07	80.65 ± 1.34	81.67 ± 2.01
P6	15	50	50	20	98.67 ± 1.05	96.54 ± 0.93	93.45 ± 1.45
P7	15	50	10	20	83.87 ± 1.02	84.87 ± 1.34	83.56 ± 0.89
P8	15	50	30	20	90.76 ± 2.04	92.23 ± 1.56	86.57 ± 0.98

particle studies, there are two essential concerns. first is the excipient effect and composition and second is the amount of coating on the pellet. In this study, we are concerned about excipients and coating effects on pellets. Previously enteric-coated tablets and pellets, multilayer film-coated, and 3D printed gastro-resistant pellets<sup>4–6</sup> were developed to improve the effect of PPIs but these formulations provide protection only against stomach secretions but have no effect on oxidative stress produced by PPI therapy.

This study aimed to overcome omeprazole-induced oxidative stress by forming pellets using polyethylene glycol 6000 and lactose after omeprazole loading coating was done using ascorbic acid for the antioxidant effect and Eudragit L-100 for controlled release of drug in the polymeric matrix system of the pellet dosage form. Ascorbic acid (Vitamin C) plays an essential role in human nephrotoxicity and renal injury as ascorbic acid exhibits a protective effect by reducing oxygen-reactive species and reducing renal damage due to its antioxidant properties and by maintaining monooxygenase and hydroxylase enzymes.<sup>7</sup> PPIs induce vascular oxidative stress, which causes endothelial dysfunction. It also causes autophagy as a survival mechanism, which also leads to oxidative stress. Previously developed formulations provide protection against stomach secretions but do not reduce oxidative stress, so to induce an antioxidant effect, coating of ascorbic acid was done on omeprazole-loaded pellets. To the best of our knowledge, previously no such coating was done.

## 2. MATERIALS AND METHODOLOGY

**2.1. Materials.** Omeprazole (molar weight 345.5 g/mol) was a kind gift from Mass Pharma Pvt. Ltd., Lahore; Avicel (MW 324.28 g/mol) was obtained from DaeJung Chemicals South Korea; poly(ethylene glycol) grade (MW 6000), lactose (MW 342.29 g/mol), ascorbic acid (MW 176.12 g/mol), and Eudragit L-100 (MW 32 000 g/mol) were obtained from Sigma Aldrich, Germany; and calcium chloride (MW 110.98 g/mol) was obtained from BDH, England.

**2.2. Synthesis and Optimization of Omeprazole (O.P.) Pellets.** Design of experiment (DoE) was employed for the synthesis of pellets by the extrusion–spheronization process.<sup>8</sup> Central composite design (CCD), executed in Design Expert (DX), Ver 13 (Stat-Ease, Inc., Minneapolis), was used to produce a planned experimental grid. According to the DX manual, the CCD employs two factorial designs, amplified by the axial and central points, making multilevels of each factor to fit a quadratic model, using minimum runs for effectual prediction. Thus, in CCD, 1 replicate of each factorial and axial point and 2 center points using a practical  $\alpha$  value of 1.3160 was employed to acquire an experimental grid for 12 runs (Table 1 under factors header).<sup>9</sup> Briefly, according to the CCD-generated grid in Table 1, Avicel, PEG 6000, lactose, and

omeprazole were mixed in a pestle and mortar. The mixture was moistened with water (granulating fluid). The wet mass was extruded with an extruder (Mini Screw Extruder, Model MSE1014, Caleva, Dorset, England) at 90 rpm speed with a pore size of 1 mm. Spheronization was done using a spheronizer (Model 120, Caleva, Dorset, England) with a rotating plate with a regular cross-hatch geometry at 700 rpm for 5 min, and then pellets were dried in an oven at 60 °C for 7 h.

**2.3. Coating of Pellets.** An ascorbic acid coating was prepared by dissolving carboxymethyl cellulose (1% w/v), calcium chloride (0.5%), and ascorbic acid (2% w/v) in distilled water at 85 °C until a clear solution was obtained; glycerol (2.5 mL/100 mL) was added as a plasticizer. The O.P.-loaded pellets were dipped in glycerol for 4 min and then dried.<sup>10</sup> For Eudragit L-100 coating, 5% w/v solution was prepared in distilled water; the pellets were dipped in the solution for 5 min and then dried.

**2.4. Characterization.** **2.4.1. Determination of Drug Loading and Encapsulation Efficiency.** To evaluate drug loading and encapsulation efficiency, 20 mg of O.P.-loaded pellets were dissolved in 2.0 mL (95% ethanol) of solution and stirred for 20 min at 100 rpm, and 3 mL of phosphate buffer solution (pH 7.4) was added after mixing in dichloromethane solution. The solution was stirred for 4 h at 300 rpm to evaporate the organic solvent. The solution was centrifuged for 30 min at 12 000 rpm and then analyzed using a U.V. spectrophotometer at 300 nm.<sup>11</sup> Drug concentration was calculated using the standard omeprazole calibration curve, and drug loading and encapsulation efficiency were calculated using the following formula:

$$\% \text{ entrapment efficiency} = \frac{\text{amount of drug in pellets}}{\text{actual amount}} \times 100 \quad (1)$$

$$\% \text{ drug loading} = \frac{\text{amount of drug in pellets}}{\text{amount of pellets}} \times 100 \quad (2)$$

**2.4.2. Micrometric Analysis.** The angle of repose was used to evaluate the flow characteristics of pellets. For this purpose, pellets were poured through a conical funnel, forming a heap at a specific level and measuring the angle between the flat surface and the horizontal plane. For bulk density, O.P.-loaded pellets were poured into a 25 mL measuring cylinder, and the weight ( $W$ ) and volume ( $V_1$ ) of pellets were measured. The measuring cylinder was tapped until the pellets reached the minimum volume ( $V_2$ ). Carr's Index and Hausner's ratio of O.P.-loaded pellets were calculated from bulk density and tapped density.<sup>12</sup> Mathematical expressions for an angle of repose, bulk and tapped density, Carr's Index, and Hausner's ratio are as follows

$$\text{bulk density} = W/V_1 \quad (3)$$

$$\text{tapped density} = W/V_2 \quad (4)$$

$$\text{Hausner's ratio} = (\text{tapped density})/(\text{bulk density}) \quad (5)$$

$$\text{Carr's index} = (\text{tapped density} - \text{bulk density}) \times 100 \quad (6)$$

**2.4.3. Structural Characterization.** The chemical relation between excipients and OP was assessed by FTIR ( $\alpha$  Bruker Platinum ATR, Germany) analysis. Surface morphology and cross-section of uncoated and dual-coated pellets were analyzed by scanning electron microscopy (SEM) analysis (Hitachi Model S, 3400N Japan). Thermal analysis was assessed by differential scanning calorimetry (DSC) at a heating rate of 10 °C/min and for 40 mL/min under a nitrogen flow using a thermogravimetric analysis instrument (Software; universal analysis, version 4.5 USA model Q600 series). The crystallinity of the pellets was determined by X-ray diffraction analysis using XRD; Siemens diffractometer model D5000, with a Cu K $\alpha$  40 kW tube and a current of 40 mA.

**2.4.4. Erosion Studies.** Erosion studies were performed using USP apparatus I (basket apparatus). 500 mL of phosphate buffer solution of different pH values (1.2 and 7.8) was used, temperature was kept at 37  $\pm$  0.05 °C at 100 rpm. Erosion was determined by removing the pellets after different intervals (15, 30, 45, and 60 min), drying the sample, and weighing.<sup>13</sup>

**2.4.5. Particle Size Distribution.** Particle size analysis of uncoated and dual-coated omeprazole pellets was done by using a vibratory sieve shaker (Vin system, Model; AS 200 digit, Retsch, Germany), and the average particle size was calculated.

**2.4.6. Cytotoxicity Analysis.** Cytotoxicity analysis was done using the 3-(4,5-dimethylthiazol-2-yl)-2,5-diphenyltetrazolium bromide (MTT) assay. HepG2 cells were harvested in 96-well plates in 100  $\mu$ L of the medium. After 24 h of incubation, the medium was replaced with 100  $\mu$ L of medium containing the tested agents at concentrations of 1, 10, 25, and 50  $\mu$ g/mL and 0.4% DMSO. The plates were incubated at 37 °C in a humidified incubator with 5% CO<sub>2</sub> for 48 h. After incubation, media were discarded, and cells were washed first with PBS. Then, 200  $\mu$ L of MTT solution and 100  $\mu$ g/mL fresh medium were added to each plate. Then the mixture was incubated for 4 h to convert MTT to formazan. After that the supernatant was aspirated and 200  $\mu$ L of DMSO was added to dissolve the formazan<sup>14</sup> then different concentrations of coated pellets were incorporated. After 24 h 0.5 mg/mL of reagent (MTT) was added to the cell medium and incubated for 90 min at 37 °C. Formazan crystals were then dissolved in dimethyl sulfoxide (DMSO), and the absorbance was recorded at 595 nm wavelength.<sup>15</sup>

**2.5. In vitro Release Studies. 2.5.1. Dissolution Studies.** *In vitro* dissolution studies were carried out using USP apparatus II. Briefly, uncoated and dual-coated pellets containing 20 mg of omeprazole were first placed in 900 mL of 0.1 N HCl solution for 2 h, then the sample then the sample with phosphate buffer of pH 6.8, the temperature was maintained at 37  $\pm$  0.5 °C, while the speed was kept at 100 rpm.<sup>4</sup> 5 mL of samples were drawn and replaced with buffer solution after regular intervals. All samples were taken from a zone midway between the surface of the medium and the top of the rotating blade and not less than 1 cm from the vessel

wall and filtered through a 0.45  $\mu$ m membrane. The solution was diluted, and absorbance was measured at 301 nm by using a UV spectrophotometer.

**2.6. Animal Studies. 2.6.1. Experimental Design.** All animal studies were done after approval from the institutional ethical committee (Ref No. 251/PEC/2023 dated 30.03.2023) following NICE godliness. A total of 24 white male healthy albino mice (BALB/c) weighing 24  $\pm$  0.25 g, 6–7 weeks old, provided a natural cycle of day and night with free access to laboratory food and water. Any injured or underweight animals were excluded from the study. To evaluate omeprazole-induced acute kidney disease, animals were divided into groups M1, M2, M3, and M4 (6 mice in each group). The M1 group consists of nude animals, the M2 group received pure O.P. 40 mg/kg/day/oral, and the M3 and M4 groups received Eudragit-coated O.P. pellets and dual-coated O.P. pellets, respectively.

**2.6.2. Histopathological Analysis.** To evaluate the drug-induced nephrotoxicity effect, all animals were sacrificed after anesthesia (pentobarbital 60 mg/kg intraperitoneally). Kidney organs were isolated and embedded in 10% formalin, then dipped in acetone for 6 h and further stained using Hematoxylin and Eosin stains (H&E stains).<sup>16</sup> The slides were prepared by using a Microtome apparatus and then studied under a microscope.

**2.6.3. Biochemical Analysis.** Blood samples (1.5 mL each) were drawn from all animals via the tail vein on the 21st day. These samples were centrifuged at 25 rpm for 15 min to obtain serum. Uric acid reagent was added to the serum. Blood samples for creatinine measurements were prepared in the same way and then, the serum uric and creatinine levels were determined using the Microlab 300 model.

**2.6.4. General Animal Evaluation. 2.6.4.1. Assessment of Bodyweight, Appetite, Feces Weight, and Urine Output.** All animals were kept in separate cages to evaluate different parameters. All animals' bodyweight, feces, and urine output were weighed and assessed before the start of the experiment, after every 7 days during the total course of the study, by using an electronic balance. The feed and water intake of all animals was monitored daily.

**2.6.4.2. Behavioral Inspection of Animals.** The behavior of all animals was inspected daily for up to 1 h before and after dosing to analyze any sign of discomfort during the study period. Anxiety levels among all groups were analyzed using the open-field test for 30 min on the 21st day.<sup>17</sup> Acute depression was studied using a tail suspension test for 5 min on the 21st day.<sup>18</sup> Cognitive function was analyzed using the novel object recognition test for up to 30 min on the 21st day.

**2.7. Molecular Docking Methodology.** The decision to choose antioxidant and anti-inflammatory proteins as target proteins was based on their significant biological properties. The protein structure of urate oxidase from *Aspergillus flavus* complexed with oxonic acid having the PDB ID 1R4U with a resolution of 1.65 Å and the structure of celecoxib bound at the COX-2 active site with PDB ID 3LN1 with a resolution of 2.40 Å was obtained from the RCSB website (<https://www.rcsb.org/>). Only chains that contained cocrystallized ligands were selected, while any undesired chains were excluded.

The Protein Preparation Wizard module of the Maestro platform<sup>19</sup> was utilized for the refinement of the protein structure during preprocessing. The tasks involved in this process encompassed the assignment of bond orders, the

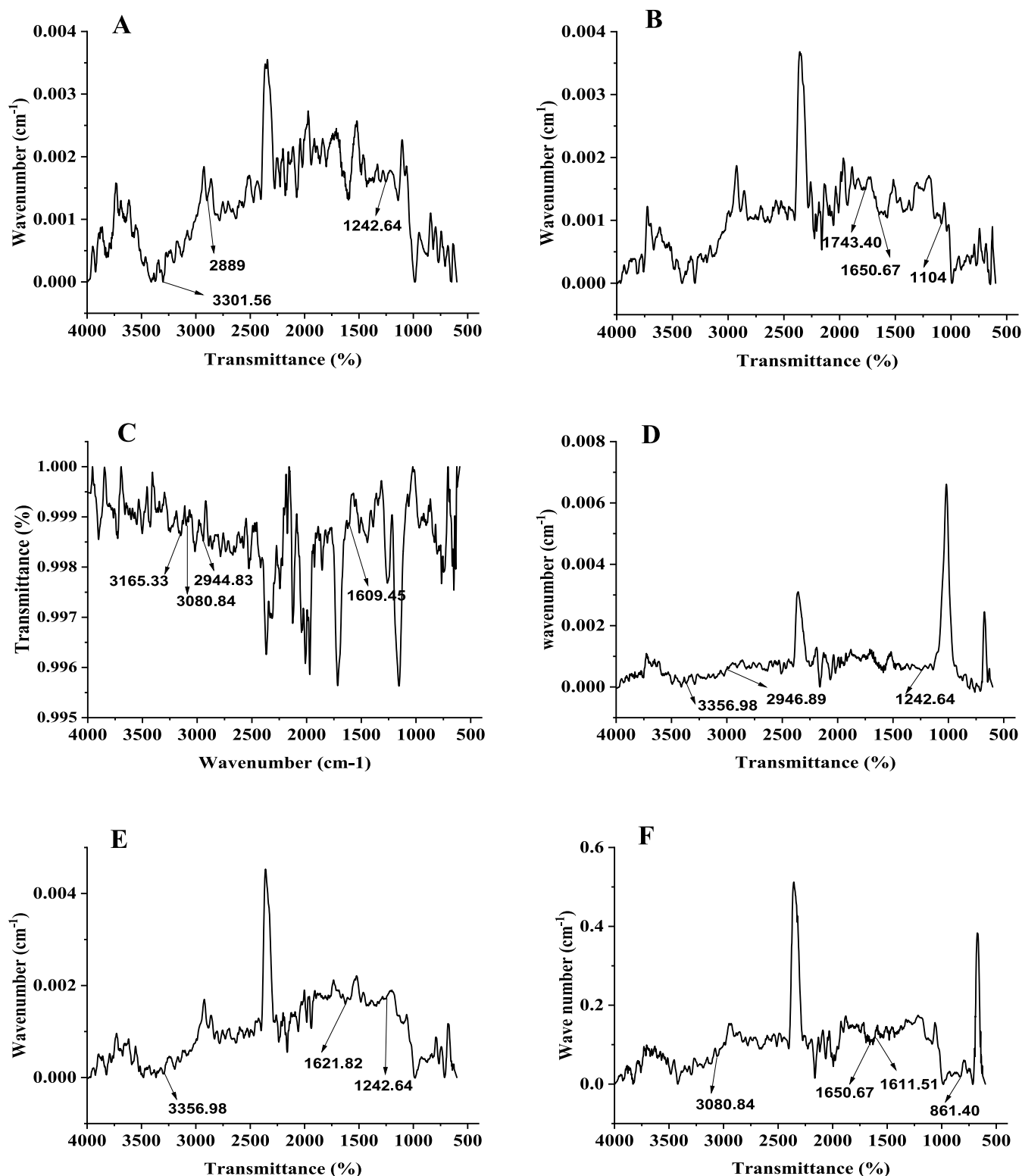


**Figure 1.** FTIR spectra of PEG 6000 (A), ascorbic acid (B), Eudragit L-100 (C), omeprazole (D), uncoated O.P.-loaded pellets (E), and coated O.P.-loaded pellets (F).

addition of hydrogen atoms, the establishment of zero-order bonds to metals and disulfide bonds, the conversion of selenomethionines to methionine, and the completion of missing side chains. The OPLS4 force field optimized structure was achieved using hydrogen bond optimization and energy minimization techniques.

The preprocessing of ligand structures involved retrieving three-dimensional structural data files (3D SDF) from the PubChem database for the target ligands ascorbic acid and omeprazole. The LigPrep module was employed to prepare the ligand structures. These structures were then subjected to energy minimization using the OPLS4 force field,<sup>20</sup> generating 32 distinct stereoisomeric and tautomeric states.

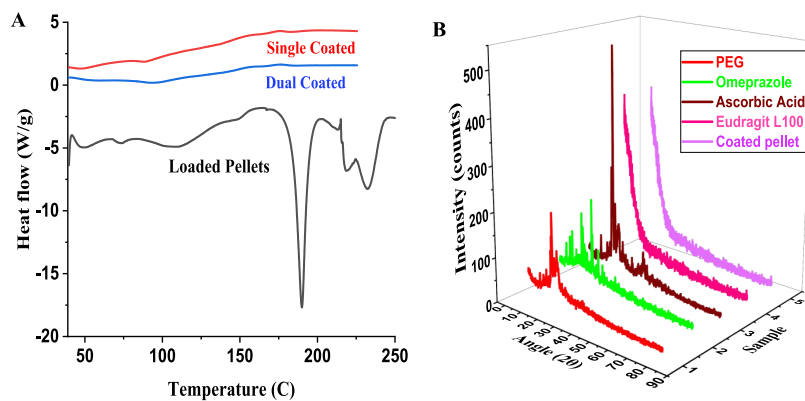


**Figure 2.** DSC analysis of uncoated and single-coated and dual-coated O.P.-loaded pellets (A). XRD comparative graph of PEG 6000, omeprazole, ascorbic acid, Eudragit L-100, and dual-coated O.P.-loaded pellets (B).

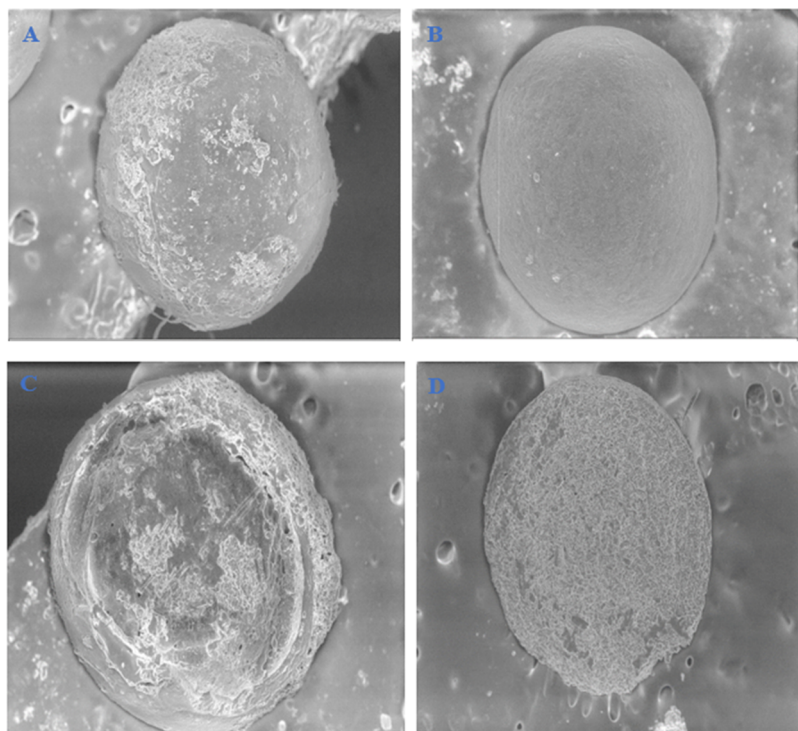


**Figure 3.** Morphological structure of the (A) uncoated O.P.-loaded pellet, (B) dual-coated O.P.-loaded pellet, (C) cross-section of uncoated O.P.-loaded pellet, and (D) cross-section of dual-coated O.P.-loaded pellet.

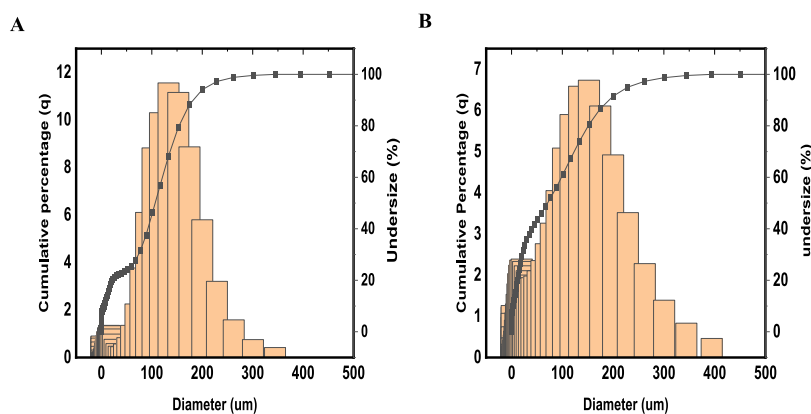


**Figure 4.** Particle size analysis of uncoated O.P.-loaded pellet (A) and dual-coated O.P.-loaded pellet (B).

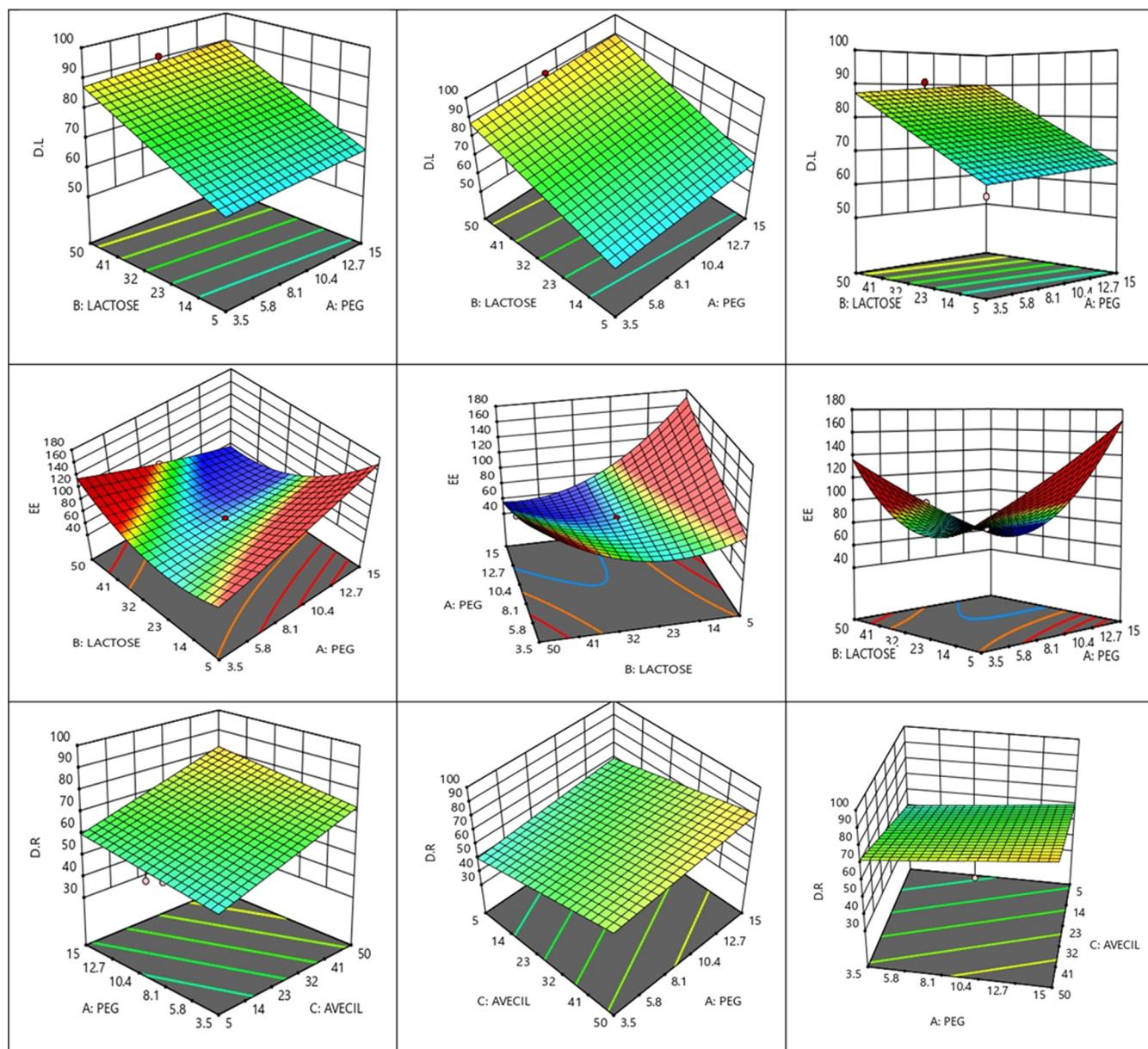


**Figure 5.** Combined effects of PEG 600, Avicel, and lactose on the characteristics of pellets.

The docking process involved the utilization of the Glide docking<sup>19,21</sup> module within the Maestro platform for docking target proteins and ligand molecules. The Glide XP (extra precision) mode was utilized for this purpose. The XP pose viewer facilitated the examination of ligand–protein interactions and the identification of the most favorable pose. The ligand interaction module generated a 2D interaction diagram of the ligand–protein complex. The obtained XP pose was further analyzed to better understand the interaction dynamics between ligand molecules and target proteins during binding. The docked complexes were validated using suitable statistical methods, such as root-mean-square deviation (RMSD) calculations, Glide binding energy, and Glide G-score.<sup>19</sup>

### 3. RESULTS AND DISCUSSION

This study fabricated various formulations using different PEG 6000, lactose, and Avicel concentrations. The % drug loading of all the formulations ranges from  $56.34 \pm 1.10$  to  $98.67 \pm$

$1.05$ , encapsulation efficiency was  $70.98 \pm 0.96$ – $98.67 \pm 1.05\%$ , and percent drug release was  $36.56 \pm 1.34$ – $93.45 \pm 1.45\%$  (Table 1). The solubility of formulation increased as the concentration of PEG 6000, Avicel, and lactose increased, increasing pores and cracks due to which more drugs were released from pellets.<sup>22–24</sup> Based on drug loading, encapsulation efficiency, and drug release results, the P6 formulation was selected as an optimal formulation and further used for coating.

**3.1. Micrometric Analysis of Pellets.** Various parameters like Hausner's ratio, Carr's index, angle of repose, tapped density, and bulk density for O.P.-loaded pellets were calculated and are shown in Table S1. Ideal values for Hausner's ratio and Carr's index are  $<1.20$  and  $\leq 15\%$ , respectively, and the angle of repose is  $\leq 25$ , indicating the free flow of the material. Hausner's ratio values range from  $1.026 \pm 0.05$  to  $1.065 \pm 0.02\%$  and Carr's index values range from  $2.3 \pm 0.07$  to  $6.1 \pm 0.06$  g/mL. These results showed that O.P.-loaded pellets have good flowing properties.

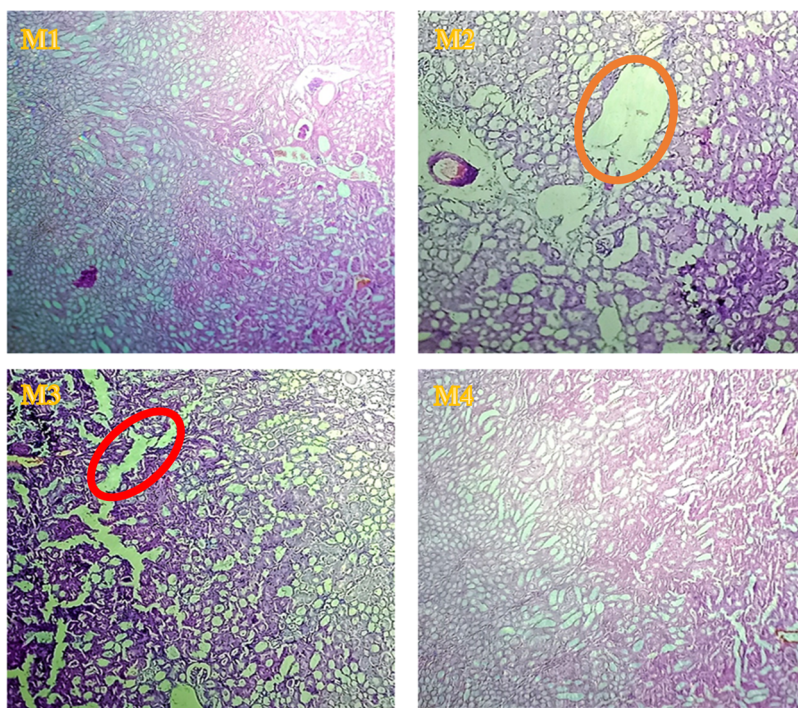


**Figure 6.** Histopathological studies of kidneys of different animal groups M1; untreated (normal) showed normal cells, M2; pure O.P. (the brown circle shows necrosis) M3; single-coated O.P. (the red circle shows necrosis of cells)-loaded pellet, M4; and dual-coated, O.P.-loaded pellet (normal cells).

### 3.2. Fourier Transform Infrared (FTIR) Spectroscopy.

The I.R. spectrum (Figure 1) of PEG 6000 showed peaks at 3300–3600, 2889, 1242.64, and 1100.05  $\text{cm}^{-1}$  attributed to O–H stretching, C–H stretching of the  $\text{CH}_2$  group, O–H stretching, and C–H deformation, respectively. Pure omeprazole showed peaks at 3356.98, 2946.89, 1617.70, and 1242.64  $\text{cm}^{-1}$  due to stretching vibration of the N–H band, N–H deformation band, and C=N and S=O bonds. Eudragit L-100 revealed peaks at 3165.33, 3080.84, 2944.83, and 1609.45  $\text{cm}^{-1}$  due to the –OH group, aromatic and aliphatic C–H stretching, and C=O group, respectively. Ascorbic acid spectra presented peaks in the range of 3215–3520  $\text{cm}^{-1}$  for the hydroxyl group, 1743.408  $\text{cm}^{-1}$  for the C=O stretching of the lactone ring, peaks at 1650.67, 1104, 863.46, and 814.002  $\text{cm}^{-1}$  represent C=C, C–O–C, C–C ring, and O–H stretching, respectively, by the previous literature.<sup>25–28</sup> The formation of PEG and lactose pellets containing O.P. showed peaks at 3356.98, 1621.82, and 1242.64  $\text{cm}^{-1}$  confirming the loading of O.P. and no chemical interaction between polymers and drug. Ascorbic acid coating is established by the presence of peaks at 861.40, 1650.67, and 1747.40  $\text{cm}^{-1}$ , and Eudragit coating is confirmed by 3080.84 and 1611.51  $\text{cm}^{-1}$  peaks. These peaks confirm the dual coating of the pellets without any chemical change.

**3.3. Thermal Analysis.** DSC analysis (Figure 2A) of O.P. loaded pellets revealed that the stability of omeprazole was enhanced by using excipients from 155 to 190 °C as pellets show a major exothermic peak at 190.04 °C due to the degradation of omeprazole. Thermal stability further increases after single and dual coating of pellets as single Eudragit L-100 coated pellets showed an endothermic peak at 189 °C due to the melting of Eudragit L-100 while pellets coated with ascorbic acid and Eudragit L-100 do not show major thermal transition due to lack of crystallinity or high melting

temperature of coating agents. The same behavior was reported previously.<sup>29</sup>

**3.4. X-ray Diffraction (XRD).** The XRD pattern (Figure 2B) of PEG 6000 showed major peaks at 19.318 and 23.328° and a few minor peaks at 26.408, 36.288, 39.748, and 45.228°. Omeprazole showed major peaks at 9.54, 12.482, 18.991, 22.435, and 28.97°. The diffraction pattern of ascorbic acid showed the polycrystalline nature with significant intense peaks at 25.27, 28.06, 29.98, 34.77, and 42.78°. Eudragit L-100 showed an amorphous nature with no prominent peaks. These agree with the reported XRD results in previous studies.<sup>30–33</sup> Single-coated (Eudragit L-100) and dual-coated (ascorbic acid and Eudragit L-100) pellets diffraction patterns revealed the amorphous nature, enhancing the pellets' stability and successful coating.

**3.5. Pellet Morphology.** SEM images (Figure 3A–D) showed that coating smooth surfaces with no visual deformation is spherical and discrete. At the same time, uncoated pellets had a spherical morphology with rough surfaces. Cross-section examination showed uniform spreading of the coating material over the pellet's surface.

**3.6. Particle Size Analysis.** Particle size analysis showed a nonsignificant increase in pellet size after coating. Omeprazole-loaded pellets had a mean size of  $85.31 \pm 77.43 \mu\text{m}$  with a median size of  $70.75 \mu\text{m}$  (Figure 4A), while dual-coated omeprazole pellets showed a mean size of  $101.99 \pm 65.56 \mu\text{m}$  with a median size of  $106.42 \mu\text{m}$  (Figure 4B).

**3.7. Erosion Studies.** Erosion studies of dual-coated pellets reveal that at acidic pH (1.2), the pellets remain intact, showing minor swelling even after 60 min, indicating minor or no drug release at acidic pH, while in basic pH (7.4), pellets split into fragments after swelling within 60 min and drug release in the basic environment (Figure S1). Obstruction in drug release in the acidic phase (pH 1.2) can be best achieved

**Table 2. Antioxidant Target Protein Structure of Urate Oxidase from *A. flavus* Complexed with Oxonic Acid Having PDB ID 1R4U Docking with Target Ligands, Interacting Amino Acid Residues, Types of Interactions, Distance in Angstrom, and Glide Score in kcal/mol**

1R4U docking with ligand	residues	type of interaction	distance (Å)	glide G-score (kcal/mol)
1R4U – ascorbic acid	HIS104	hydrogen bond	2.262	−5.5
	HIS104	hydrogen bond	1.872	
	ARG105	hydrogen bond	3.665	
1R4U – omeprazole	THR107	hydrogen bond	2.923	−6.9
	ARG108	hydrogen bond	2.013	
	ARG108	hydrogen bond	2.425	
	ARG128	hydrogen bond	2.651	
	ARG108	hydrogen bond	2.754	
	THR107	hydrophobic	3.641	
	PRO76	hydrophobic	4.229	
	CYS103	hydrophobic	3.933	
	ARG128	hydrophobic	4.516	
	ARG108	hydrophobic	4.886	
1R4U – reference drug (oxonic acid)	ARG176	hydrogen bond	2.316	−5.3
	HIS256	hydrophobic	4.639	
	ARG176	hydrogen bond	2.057	
	ARG176	hydrogen bond	1.896	
	VAL227	hydrogen bond	1.915	
	GLN228	hydrogen bond	2.191	
	ASN254	hydrogen bond	2.800	
	ASN254	hydrogen bond	2.681	
	GLN228	hydrogen bond	3.106	
	HIS256	hydrogen bond	3.535	
	ASN254	hydrogen bond	3.273	
	PHE159	hydrophobic	3.835	

due to the coating of ascorbic acid and Eudragit that shields omeprazole in an acidic environment and inhibits drug release in the stomach.

**3.8. Cell Viability Studies.** Cell viability (Figure S2) was found to be 89–97% at different concentrations (0.02–0.2 mg) of coated pellets, confirming the safe and nontoxic effect of the formulation. All the polymers used in the formulation are natural, biodegradable, and nontoxic.

**3.9. In Vitro Drug Release Studies.** *In vitro* dissolution studies of uncoated and coated pellets showed that for the first two hours in an acidic environment (pH 1.2), omeprazole release from single- and dual-coated pellets was below 20%. This decrease in drug permeability and drug release was due to polymers used for coating that exhibit gastric resistance and no drug release in the acidic environment. At pH 6.8, drug release was about 99.54% in the next 8 h. The drug release at this pH

was due to the breakdown of the polymeric complex and the release of maximum amount of the drug as partially soluble ions in the dissolution media as shown in Figure 5.

**3.10. In Vivo Studies.** *In vivo*, a biocompatibility test was performed on 4 mice divided into 2 groups. Blank pellets were given to group 1 and drug-loaded pellets were given to group 2 and no toxicity was observed in any of the mice, furthermore, no mice died during the complete animal studies indicating biocompatibility of for formulation.

**3.10.1. General Evaluation.** During the animal studies, no difference was observed in the fur of all animals. M1 and M4 animals had an average increase in weight from  $24 \pm 0.25$  g to  $40 \pm 0.14$  g, while animals of groups M2 and M3 showed an average decrease in weight from  $34 \pm 0.3$  to  $29 \pm 0.2$  g after 14 days. This change could be attributed to renal injury. The glomerular filtration rate (GFR) falls below normal due to renal disease, leading to less appetite, which in turn causes weight loss, as indicated in the literature.<sup>34</sup> Group M2 and M3 showed a drop in food intake ( $3.2 \pm 0.4$  g/day) as compared to M1 and M4 ( $5.6 \pm 0.3$  g/day). This loss of appetite is a symptom of AKI and is related to low acyl-ghrelin levels and high TNF- $\alpha$  and IL-6, while groups M1 and M4 showed constant appetite. Furthermore, the water intake of group M2 and M3 animals showed a decline ( $1.9 \pm 0.2$  mL/day) compared with M1 and M4 ( $4.5 \pm 0.3$  mL/day).

**3.10.2. Behavioral Inspection.** The behavioral activity of M1 and M4 remained normal throughout the study. In contrast, M2 and M3 were found to be less energetic and fatigued since day 14. This fatigue is related to decreased oxygen delivery and a rise in anaerobic metabolism, a sign of nephrotoxicity, AKI. Thigmotaxis is used as an index for anxiety-associated behavior in mice in open-field tests (Figure S4). The animals of groups M2 and M3 spent  $26.5 \pm 0.9$  min near the maze walls and showed low locomotor activity, displaying anxiogenic behavior. Meanwhile, the mice of groups M1 and M4 transverse the inner zones of the maze at a much higher frequency and spend less time at  $12 \pm 0.5$  min near the maze walls, indicating healthy behavior. The same anxiogenic behavior was also reported in AKI-induced mice models.<sup>35</sup>

In the tail suspension test (Figure S4), the mice of groups M2 and M3 ceased the escape-related behavior. They developed the immobile posture earlier ( $1.2 \pm 0.1$  min) than M1 and M4 ( $3.5 \pm 0.2$  min), indicating depression-like behavior. Similar depressive behavior was also previously associated with AKI.<sup>36</sup>

In the novel object recognition test, all the animals displayed an innate preference for the novel object rather than the familiar object, indicating normal cognitive function with no signs of memory loss. Higher anxiogenic and depressive-like behavior is a symptom of AKI, as renal tubular necrosis leads to accumulated uremic toxins causing stress and anxiety.

**3.10.3. Feces and Urine Output Variations.** M1 (normal), M3, and M4 group's feces weight ranged from 19 to  $22 \pm 1$  mg/day as compared to the M2 group, which was  $8 \pm 1$  mg/day, representing constipation in animals of group M2, a well-established adverse effect of PPIs. Meanwhile, M3 and M4 were less affected by this adverse effect owing to the laxative properties of polymers.

A nonsignificant drop in urine volume in groups M2 and M3 ( $0.5 \pm 0.1$  mL/day) was observed on the 21st day compared to groups M1 and M4 ( $1.4 \pm 0.1$  mL/day), as shown in Table S2. Less urine output is a symptom of AKI discussed in the literature previously.<sup>37</sup>

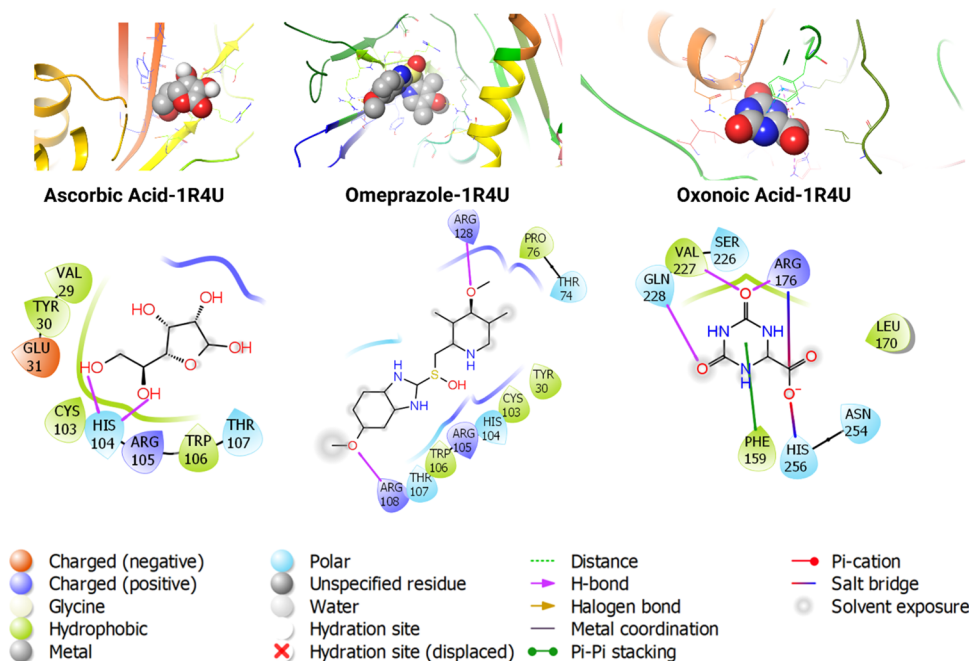


**Figure 7.** Docked and 2D view of the structure of urate oxidase from *A. flavus* complexed with oxonic acid having PDB ID 1R4U antioxidant protein with the target ligands ascorbic acid and omeprazole.

**3.10.4. Serum Uric Acid Test.** In animals of groups M2 and M3, average serum uric acid levels were elevated at  $4.8 \pm 0.2$  and  $4.6 \pm 0.1$  mg/dL, respectively, indicating hyperuricemia in both groups compared to the positive control group M1 ( $2.2 \pm 0.3$  mg/dL). Group M4 showed serum uric acid levels of  $2.6 \pm 0.1$  mg/dL within the normal range. This rise in serum uric acid levels of groups M2 and M3 was due to stress and maximum reabsorption of uric acid by the proximal renal tubule, which is a clear indication of renal tubular cell death leading to a fall in GFR, which is the indication of AKI, as reported previously.<sup>38</sup>

**3.10.5. Serum Creatinine Test.** Groups M2 and M3 showed elevated serum creatinine levels ( $0.4 \pm 0.02$  mg/dL) compared to those of M1 (positive control) and M4 ( $0.2 \pm 0.03$  mg/dL), as shown in Table S2. This rise in creatinine represents a decline in renal clearance due to necrotic tubular cell death leading to AKI, as reported<sup>39</sup>

**3.10.6. Histopathological Studies.** Histopathological studies of mice renal tissues of groups M2 and M3 showed tubular luminal dilatation and coagulative necrosis, indicating loss of epithelial nuclei attributed to acute tubular injury (ATI). Furthermore, a ghost-like tubular appearance appeared in dark pink on (H&E) staining, exhibiting acute kidney injury (AKI). The SOP degree of loss in the brush border was also seen (Figure 6). The same necrotic effect was reported, while renal cells of groups M1 and M4 had a normal volume of epithelial cells with no loss of nuclei. Additionally, brush borders appeared normal, with no signs of necrosis. These studies confirmed that a 40 mg/kg/day dose of omeprazole caused ATI, which is responsible for AKI. Meanwhile, the coating of ascorbic acid and Eudragit L-100 on the O.P. pellets inhibits the mechanism of AKI by diminishing mitochondrial and cytosolic ROS production and reducing lipid peroxidation, inhibiting necrotic tubular cell death.

**3.11. In Silico Docking Results.** Table 2 displays the results of molecular docking experiments conducted on the protein structure of urate oxidase from *A. flavus* complexed

with oxonic acid having PDB ID 1R4U with three distinct ligands: ascorbic acid, omeprazole, and a reference drug known as oxonic acid. These experiments aimed to better investigate the interactions between the ligands and the target protein to understand their binding affinities and potential as therapeutic agents.

Regarding ascorbic acid, it establishes hydrogen bond interactions with the protein's essential residues HIS104 and ARG105. These interactions exhibit short distances, which suggests a high degree of binding. A negative Glide G-score of  $-5.5$  kcal/mol provides additional evidence of a strong binding affinity.

In contrast, omeprazole exhibits a broader range of interactions with 1R4U. The molecule shows a robust binding profile, as it engages in hydrogen bonding interactions with THR107, ARG108, and ARG128. Moreover, the favorable binding of the ligand is further enhanced by hydrophobic interactions involving PRO76 and CYS103. The binding interaction is highlighted by a relatively low Glide G-score of  $-6.9$  kcal/mol.

The reference drug, oxonic acid, demonstrates several hydrogen bonding interactions with residues including ARG176, HIS256, VAL227, GLN228, ASN254, and PHE159 within the 1R4U structure. In addition, hydrophobic interactions are also involved. Based on the Glide G-score of  $-5.3$  kcal/mol, it can be inferred that oxonic acid exhibits favorable binding to the protein. However, it is worth noting that its binding affinity is slightly lower than omeprazole. All the results are shown in Figure 7. The results underscore the significance of comprehending these interactions on a molecular level to develop more efficacious pharmaceuticals for antioxidant applications.

Table 3 provides a comprehensive summary of the outcomes derived from molecular docking simulations conducted on the protein structure of celecoxib bound at the COX-2 active site with PDB ID 3LN1 having 3NL1 in conjunction with three distinct ligands: ascorbic acid, omeprazole, and a reference

**Table 3. Anti-Inflammatory Target Protein Structure of Celecoxib Bound at the COX-2 Active Site with PDB ID 3NL1, Docking with Target Ligands, Interacting Amino Acid Residues, Types of Interaction, Distance in Angstroms, and Glide Score in kcal/mol**

3NL1 docking with ligand	residues	type of interaction	distance (Å)	glide G-score (kcal/mol)
3NL1 – ascorbic acid	VAL214	hydrogen bond	2.238	−5.7
	ASN523	hydrogen bond	3.053	
	ASN523	hydrogen bond	2.360	
	ASN361	hydrogen bond	2.095	
	GLY519	hydrogen bond	2.419	
3NL1 – omeprazole	TYR134	hydrogen bond	2.902	−7.3
	THR198	hydrogen bond	2.256	
	THR198	hydrogen bond	2.419	
	ASN368	hydrogen bond	2.101	
	HIS193	electrostatic	4.070	
	HIS193	electrostatic	4.095	
	HIS200	electrostatic	4.677	
	HIS372	electrostatic	3.992	
	HIS200	hydrophobic	3.736	
	HIS372	hydrophobic	4.169	
	HIS372	hydrophobic	4.199	
	HIS200	hydrophobic	4.832	
	HIS374	hydrophobic	4.268	
	3NL1 – reference drug (celecoxib)	GLN189	hydrogen bond	
GLN189		hydrogen bond	2.694	
THR198		hydrogen bond	2.017	
HIS200		hydrogen bond	2.652	
ASN368		hydrogen bond	2.884	
GLN440		hydrogen bond	2.403	
HIS193		electrostatic	3.665	
HIS200-S		other	5.549	
HIS372-S		other	4.461	
HIS193		hydrophobic	4.484	
LYS197		hydrophobic	4.375	
ARG208		hydrophobic	4.477	
VAL277		hydrophobic	4.776	
LYS197		hydrophobic	5.170	
VAL277		hydrophobic	4.756	
HIS193	hydrophobic	4.805		

drug known as celecoxib. These simulations comprehensively understand the binding interactions, distances, and binding affinities between the ligands and the target protein.

Regarding ascorbic acid, it establishes hydrogen bond interactions with multiple residues within the 3NL1 protein, namely, VAL214, ASN523, ASN361, ASN523, and GLY519. The observed interactions are relatively short distances, indicating a high affinity between the ligand and the protein. The Glide G-score of −5.7 kcal/mol provides additional

evidence of the strong binding affinity between ascorbic acid and 3NL1.

The compound omeprazole establishes diverse interactions upon binding to protein 3NL1. The interactions observed in the system involve hydrogen bonds formed with TYR134, THR198, THR198, ASN368, HIS193, HIS193, HIS200, HIS372, HIS200, HIS372, HIS372, HIS272, HIS200, and HIS374. Furthermore, there are electrostatic and hydrophobic interactions at play. The distances between the atoms involved in the interaction exhibit variation, yet they consistently fall within an acceptable range. Based on a Glide G-score of −7.3 kcal/mol, there is a notable indication of a robust binding affinity between omeprazole and 3NL1.

The reference drug, celecoxib, forms hydrogen bonding interactions with amino acid residues GLN189, THR198, HIS200, ASN368, GLN440, and HIS193. Electrostatic forces engage HIS200-S and HIS372-S. Additionally, there have been observations of hydrophobic interactions with LYS197, ARG208, and VAL277 amino acids. The distances associated with these interactions fall within a favorable range. The calculated Glide G-score of −7.4 kcal/mol suggests a significant binding affinity between the reference drug and 3NL1. All the results are shown in Figure 8.

The incorporation of ascorbic acid in the experimental study is consistent with the findings obtained from the *in silico* docking analysis. Both the experimental and computational data demonstrate the antioxidant properties of ascorbic acid. During the experimental phase, the objective was to apply a coating of ascorbic acid to the pellets to mitigate oxidative stress. The docking results obtained through computational methods for proteins 1R4U and 3NL1 reveal robust hydrogen bonding interactions with ascorbic acid, suggesting its potential as an antioxidant. The correlation highlights the significance of molecular docking in predicting binding affinities between compounds, such as ascorbic acid, and target proteins. This validation further supports its utility in experimental design.

The study also included the pharmaceutical agent known as omeprazole. The docking results obtained for omeprazole with 1R4U and 3NL1 revealed strong binding affinities characterized by a wide range of hydrogen bonds and hydrophobic interactions. This implies that omeprazole may possess therapeutic effects beyond its primary indication, potentially associated with its interactions with antioxidant and anti-inflammatory proteins. This discovery justifies further investigation into the potential repurposing of currently available drugs for novel therapeutic purposes.

The use of reference drugs, namely, oxonic acid and celecoxib, in the study's computational components serves as a standard for comparison. The computational findings for these drugs demonstrated favorable binding affinities, albeit slightly lower than those of ascorbic acid and omeprazole for oxonic acid and slightly lower from celecoxib. The aforementioned correlation highlights the dependability of molecular docking in evaluating potential interactions between drugs and proteins and its suitability as a screening tool. This study's combined experimental and molecular docking technique sheds light on the ability of ascorbic acid and omeprazole to reduce oxidative stress and inflammation, enabling medication development and repurposing.

#### 4. CONCLUSIONS

In conclusion, this study provides compelling evidence supporting the effective alleviation of acute kidney infection

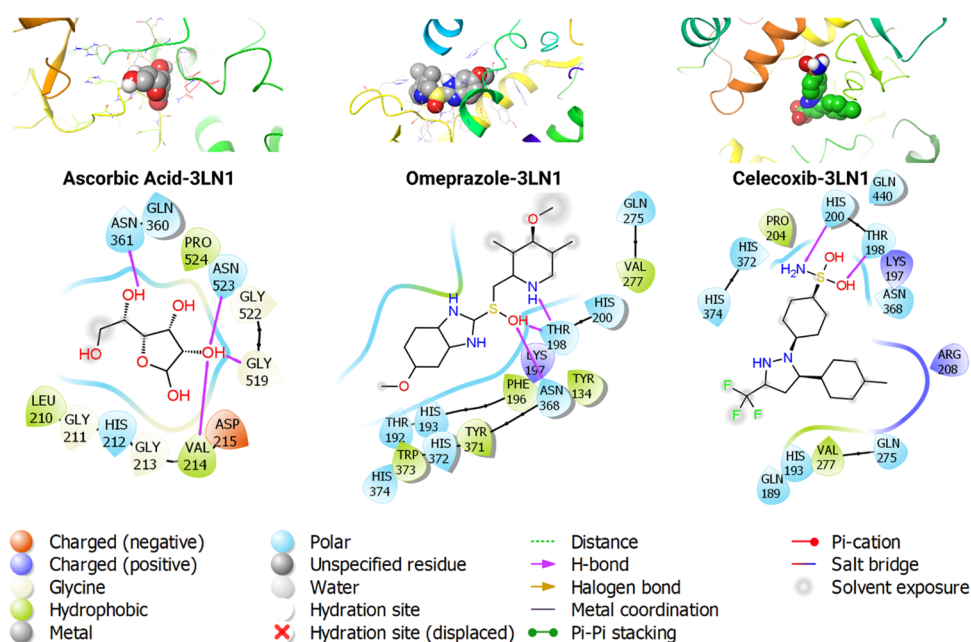


**Figure 8.** Docked and 2D view of the structure of celecoxib bound at the COX-2 active site with PDB ID 3LN1 anti-inflammatory protein with the target ligands ascorbic acid and omeprazole.

induced by omeprazole through the strategic application of an ascorbic acid coating, emphasizing the preventive impact attributed to the inherent antioxidant properties of ascorbic acid. The XRD analysis confirmed the crystalline nature of the coating, and thermal degradation studies revealed increased stability up to 500 °C. Cytotoxicity analysis demonstrated a nontoxic behavior of the coated pellets, with 97% cell viability. *In vitro* dissolution studies showcased controlled drug release with less than 20% at pH 1.2 and 99.54% at 6.8. Animal studies exhibited significant differences in weight, urine output, and fecal output between rodents on pure omeprazole and those on ascorbic acid pellets, suggesting a protective effect of the coating. Elevated uric acid and creatinine levels in the pure omeprazole group indicated the onset of acute kidney injury (AKI), a finding supported by histopathological studies of renal cells. The integration of experimental investigations and molecular docking not only holds promise for novel medication development but also sheds light on repurposing opportunities. Emphasizing the potential of ascorbic acid and omeprazole in mitigating oxidative stress and inflammation, these pivotal findings lay a solid groundwork for future research initiatives, showcasing the versatility of the developed carrier for application to other drugs within the proton pump inhibitors class.

## ■ ASSOCIATED CONTENT

### Data Availability Statement

The data presented in the current study are available in the Supporting Information.

### SI Supporting Information

The Supporting Information is available free of charge at <https://pubs.acs.org/doi/10.1021/acsomega.3c07396>.

Table S1 (micrometric analysis), Table S2 (animal group study), Figure S1 (erosion studies), Figure S2 (cytotoxicity analysis), Figure S3 (ramp graph for the DoE), and Figure S4 (open-field test and tail suspension test) data used for this work (PDF)

## ■ AUTHOR INFORMATION

### Corresponding Authors

**Farhan Siddique** – School of Pharmaceutical Science and Technology, Tianjin University, Tianjin 300072, P. R. China; Email: [drfarhansiddique@tju.edu.cn](mailto:drfarhansiddique@tju.edu.cn)

**Gezahign Fentahun Wondmie** – Department of Biology, Bahir Dar University, Bahir Dar 6000, Ethiopia; [orcid.org/0009-0006-2744-7373](https://orcid.org/0009-0006-2744-7373); Email: [resercherfent@gmail.com](mailto:resercherfent@gmail.com)

### Authors

**Hina Raza** – Department of Pharmaceutics, Faculty of Pharmacy, Bahauddin Zakariya University, Multan 60800, Pakistan

**Ali Abrar** – Department of Pharmaceutics, Faculty of Pharmacy, Bahauddin Zakariya University, Multan 60800, Pakistan

**Asmara Ashraf** – Department of Pharmaceutics, Faculty of Pharmacy, Bahauddin Zakariya University, Multan 60800, Pakistan

**Suryyia Manzoor** – Institute of Chemical Sciences, Bahauddin Zakariya University, Multan 60800, Pakistan

**Rahat Shamim** – Punjab University College of Pharmacy, University of the Punjab, Lahore 54000, Pakistan

**Ahmad Mohammad Salamatullah** – Department of Food Science & Nutrition, College of Food and Agricultural Sciences, King Saud University, Riyadh 11451, Saudi Arabia

**Mohammed Bourhia** – Department of Chemistry and Biochemistry, Faculty of Medicine and Pharmacy, Ibn Zohr University, Laayoune 70000, Morocco

Complete contact information is available at:

<https://pubs.acs.org/doi/10.1021/acsomega.3c07396>

### Author Contributions

Conceptualization, writing the original draft, and reviewing and editing: H.R., A. Abrar, A. Ashraf, and S.M. Formal analysis, investigations, funding acquisition, reviewing, and editing: R.S.,

F.S., and A.M.S. Resources, data validation, data curation, and supervision: F.S., M.B., and G.F.W.

### Funding

This work is financially supported by the Researchers Supporting Project number (RSP-2023R437), King Saud University, Riyadh, Saudi Arabia.

### Notes

The authors declare no competing financial interest.

## ACKNOWLEDGMENTS

All the authors are greatly thankful to the production manager Dr. Nazar Abbas “Mass Pharma Pvt. Ltd. Lahore” for his kind contribution to the supply of ingredients, omeprazole drug and ascorbic acid, and providing the facility for providing the coating optimization techniques.

## REFERENCES

- (1) Vanderhoff, B. T.; Tahboub, R. M. Proton pump inhibitors: an update. *Am. Fam. Physician* **2002**, *66* (2), 273–281.
- (2) Sachs, G.; Shin, J.; Howden, C. The clinical pharmacology of proton pump inhibitors. *Aliment. Pharmacol. Ther.* **2006**, *23*, 2–8.
- (3) Wu, A. A.; Wang, Y. I. The more monitoring, the better quality? empirical evidence from the generic drug industry. *Empirical Evidence from the Generic Drug Industry*, 2021. <http://dx.doi.org/10.2139/ssrn.3596559>.
- (4) Chakravarthy, K. K.; et al. Formulation and evaluation of enteric coated pellets of omeprazole. *Int. J. Drug Dev. Res.* **2012**, *4* (4), 257–264.
- (5) He, W.; Fan, L. F.; Du, Q.; et al. Design and in vitro/in vivo evaluation of multi-layer film coated pellets for omeprazole. *Chem. Pharm. Bull.* **2009**, *57* (2), 122–128.
- (6) Rouaz-El Hajoui, K.; Herrada-Manchón, H.; Rodríguez-González, D.; et al. Pellets and gummies: Seeking a 3D printed gastro-resistant omeprazole dosage for paediatric administration. *Int. J. Pharm.* **2023**, *643*, No. 123289.
- (7) Rapa, S. F.; Di Iorio, B. R.; Campiglia, P.; et al. Inflammation and Oxidative Stress in Chronic Kidney Disease—Potential Therapeutic Role of Minerals, Vitamins and Plant-Derived Metabolites. *Int. J. Mol. Sci.* **2020**, *21* (1), 263.
- (8) Ibrahim, M. A.; El-Badry, M. Formulation of immediate release pellets containing famotidine solid dispersions. *Saudi Pharm. J.* **2014**, *22* (2), 149–156.
- (9) Ijaz, S.; Sultana, M.; Shamim, R.; et al. Development and DoE-ANN based optimization of novel swellable matrix-diffusible doxorubicin loaded zinc oxide nanoflowers using sonochemical-precipitation method. *Int. J. Pharm.* **2023**, *633*, No. 122584.
- (10) Saba, M. K.; Sogvar, O. B. Combination of carboxymethyl cellulose-based coatings with calcium and ascorbic acid impacts in browning and quality of fresh-cut apples. *LWT – Food Sci. Technol.* **2016**, *66*, 165–171.
- (11) Rezazadeh, M.; Safaran, R.; Minaiyan, M.; et al. Preparation and characterization of Eudragit L 100–55/chitosan enteric nanoparticles containing omeprazole using general factorial design: in vitro/in vivo study. *Res. Pharm. Sci.* **2021**, *16* (4), 358.
- (12) Raza, H.; et al. Development and in vitro characterization of 5-fluorouracil loaded, colon-targeted drug delivery system. *Trop. J. Pharm. Res.* **2018**, *17*, 195.
- (13) Das, S.; et al. Preparation and evaluation of sustained release enteric coated mucoadhesive tablets of omeprazole for local action. *Res. J. Pharm. Technol.* **2008**, *1* (3), 166–170.
- (14) Su, N.-W.; Lin, Y. L.; Lee, M. H.; et al. Ankaflavin from *Monascus*-Fermented Red Rice Exhibits Selective Cytotoxic Effect and Induces Cell Death on Hep G2 Cells. *J. Agric. Food Chem.* **2005**, *53* (6), 1949–1954.
- (15) Baliharová, V.; Skálová, L.; Maas, R. F. M.; et al. The effects of mebendazole on P4501A activity in rat hepatocytes and HepG2 cells. Comparison with tiabendazole and omeprazole. *J. Pharm. Pharmacol.* **2010**, *55* (6), 773–781.
- (16) Khayyat, L. I. The histopathological effects of an electromagnetic field on the kidney and testis of mice. *Eurasia J. Biosci.* **2011**, *5*, 103–109.
- (17) Seibenhener, M. L.; Wooten, M. C. Use of the open field maze to measure locomotor and anxiety-like behavior in mice. *J. Vis. Exp.* **2015**, *96*, No. e52434, DOI: 10.3791/52434.
- (18) Can, A.; Dao, D. T.; Terrillion, C. E.; et al. The tail suspension test. *J. Vis. Exp.* **2012**, *59*, No. e3769, DOI: 10.3791/3769-v.
- (19) Friesner, R. A.; Murphy, R. B.; Repasky, M. P.; et al. Extra precision glide: Docking and scoring incorporating a model of hydrophobic enclosure for protein–ligand complexes. *J. Med. Chem.* **2006**, *49* (21), 6177–6196.
- (20) Harder, E.; Damm, W.; Maple, J.; et al. OPLS3: a force field providing broad coverage of drug-like small molecules and proteins. *J. Chem. Theory Comput.* **2016**, *12* (1), 281–296.
- (21) Friesner, R. A.; Banks, J. L.; Murphy, R. B.; et al. Glide: a new approach for rapid, accurate docking and scoring. I. Method and assessment of docking accuracy. *J. Med. Chem.* **2004**, *47* (7), 1739–1749.
- (22) Goskonda, S. R.; Hileman, G. A.; Upadrashta, S. M. Controlled release pellets by extrusion-spheronization. *Int. J. Pharm.* **1994**, *111* (1), 89–97.
- (23) Sinha, V.; Agrawal, M.; Kumria, R. Influence of formulation and excipient variables on the pellet properties prepared by extrusion spheronization. *Curr. Drug Delivery* **2005**, *2* (1), 1–8.
- (24) O'Connor, R. E.; Schwartz, J. B. Drug release mechanism from a microcrystalline cellulose pellet system. *Pharm. Res.* **1993**, *10*, 356–361.
- (25) Khan, A.; Reddy, P. Ternary solid dispersions of omeprazole for enhancing solubility and dissolution. *World J. Pharm. Res.* **2015**, *5990*, 2402–2412.
- (26) Sahu, M.; Reddy, V. R. M.; Kim, B.; et al. Fabrication of Cu<sub>2</sub>ZnSnS<sub>4</sub> Light Absorber Using a Cost-Effective Mechanochemical Method for Photovoltaic Applications. *Materials* **2022**, *15* (5), 1708.
- (27) Sreeja, V.; Jayaprabha, K. N.; Joy, P. A. Water-dispersible ascorbic-acid-coated magnetite nanoparticles for contrast enhancement in MRI. *Appl. Nanosci.* **2015**, *5* (4), 435–441.
- (28) Medradosantos, T. et al. Magnetite-loaded enteric particles: the influence of localized magnetic field on controlled release of nifedipine. *Asian J. Biochem. Pharm. Res. Drug.* **2014**.
- (29) Sharma, V. D.; Akocak, S.; Ilies, M. A.; et al. Solid-State Interactions at the Core-Coat Interface: Physicochemical Characterization of Enteric-Coated Omeprazole Pellets Without a Protective Sub-Coat. *AAPS PharmSciTech* **2015**, *16*, 934–943, DOI: 10.1208/s12249-014-0263-z.
- (30) Jayaramudu, T.; Raghavendra, G. M.; Varaprasad, K.; et al. Preparation and characterization of poly (ethylene glycol) stabilized nano silver particles by a mechanochemical assisted ball mill process. *J. Appl. Polym. Sci.* **2016**, *133*, 43027.
- (31) Al-Badr, A. Omeprazole. In *Profiles of Drug Substances, Excipients and Related Methodology*; Elsevier Inc., 2010; Vol. 35, Chapter 4, pp 151–262.
- (32) Palma, H.; Alvarez-Ramírez, J.; Vargas-Torres, A. Using modified starch/maltodextrin microparticles for enhancing the shelf life of ascorbic acid by the spray-drying method: Ascorbic acid encapsulated in modified starches to enhance shelf life. *Starch* **2018**, *70*, No. 1700323, DOI: 10.1002/star.201700323.
- (33) Sharma, M.; Sharma, V.; Panda, A. K.; et al. Enteric Microsphere Formulations of Papain for Oral Delivery. *J. Pharm. Soc. Jpn.* **2011**, *131*, 697–709.
- (34) Bruci, A.; Tuccinardi, D.; Tozzi, R.; et al. Very low-calorie ketogenic diet: a safe and effective tool for weight loss in patients with obesity and mild kidney failure. *Nutrients* **2020**, *12* (2), 333.
- (35) Liu, Y.; Yoo, M. J.; Savonenko, A.; et al. Amyloid pathology is associated with progressive monoaminergic neurodegeneration in a transgenic mouse model of Alzheimer's disease. *J. Neurosci.* **2008**, *28* (51), 13805–13814.

(36) Stallons, L. J.; Whitaker, R. M.; Schnellmann, R. G. Suppressed mitochondrial biogenesis in folic acid-induced acute kidney injury and early fibrosis. *Toxicol. Lett.* **2014**, *224* (3), 326–332.

(37) Legrand, M.; Payen, D. Understanding urine output in critically ill patients. *Ann. Intensive Care* **2011**, *1* (1), 13.

(38) Xu, X.; Hu, J.; Song, N.; et al. Hyperuricemia increases the risk of acute kidney injury: a systematic review and meta-analysis. *BMC Nephrol.* **2017**, *18* (1), 27.

(39) Lumlertgul, N.; Peerapornratana, S.; Trakarnvanich, T.; et al. Early versus standard initiation of renal replacement therapy in furosemide stress test non-responsive acute kidney injury patients (the FST trial). *Crit. Care* **2018**, *22*, 101.